Effects of microstructure on the creep properties of a new Ni-Co base superalloy

L. Xu, C.Q. Sun, C.Y Cui, C. Zhang

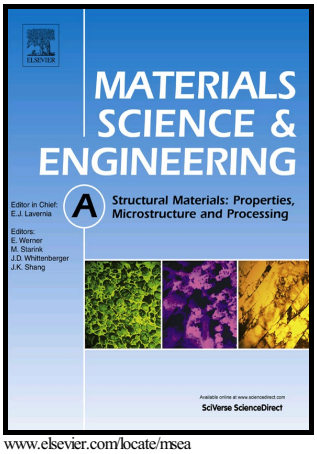

www.elsevier.com/locate/msea

PII: S0921-5093(16)31131-5
DOI: http://dx.doi.org/10.1016/j.msea.2016.09.060
Reference: MSA34145

To appear in: *Materials Science & Engineering A*

Received date: 4 July 2016
Revised date: 15 September 2016
Accepted date: 15 September 2016

Cite this article as: L. Xu, C.Q. Sun, C.Y Cui and C. Zhang, Effects o microstructure on the creep properties of a new Ni-Co base superalloy, *Material Science & Engineering A,* http://dx.doi.org/10.1016/j.msea.2016.09.060

Effects of microstructure on the creep properties of a new Ni-Co base superalloy

L. Xu[ab], C. Q. Sun[a], C. Y Cui[b*], C. Zhang[a]

a Shenyang Institute of engineering, 18 Puchang Road, Shenyang, China, 110136

b Superalloys Division, Institute of Metal Research, Chinese Academy of Sciences, 72 Wenhua Road, Shenyang, China, 110016

Abstract

The effects of microstructure on the creep behavior in a new developed Ni-Co base superalloy were investigated and two microstructures were obtained by different heat treatments. The results show that the air cooling microstructure, consisting of large spherical γ′ and small spherical γ′, resulted in a slow creep rate and small creep strain. While the slow cooling microstructure, consisting of large flowery γ′ and small spherical γ′, resulted in a fast creep rate and large creep strain. The γ channel and γ′ morphology are two main factors for these differences, the large γ channel and flowery γ′ in the slow cooling microstructure causing the dislocations slip easily in the γ matrix and cut into the γ′precipitates with low stress.

Keywords: Microstructure; creep behavior; superalloy

1 Introduction

The newly developed Ni-Co base superalloy is designed to mainly use in aero engine and the gas turbine disk. The disc rotors in the high pressure compressor accommodate higher temperatures and stresses. Therefore, the alloy must possess the inherent capacity to retain strength and resistance to creep, while the creep resistance is an important performance index for this alloy.

Alloy composition and microstructure are two important factors that determine the creep resistance of a polycrystalline Ni-base disk superalloy. Yuan et al. has investigated the effect of alloy composition on the creep mechanism at intermediate temperature in the newly developed Ni-Co base superalloys [1-3]. Their results indicate that Co content affect the stacking faults energy effectively. With higher Co content, the stacking fault energy is lower leading to a high density of deforming twin

*Corresponding author: Tel: 86-24-8397- 8292, Email: chycui@imr.ac.cn

in the deformation microstructure, which can improve the mechanical properties.

Besides alloy composition, the mechanical properties of Ni-base superalloys are influenced by the size scale and distribution of the γ′ precipitates, which is the prime strengthening constituent in Ni-base superalloys. The effect of γ′ distribution on the creep deformation has been investigated by Locq et al. in NR3 at 700 °C and 500, 650 MPa [4]. The results show that the creep rate is much more rapid with a monomodal γ′ size distribution and it deforms by way of a/2<110> dislocation in a climb/bypass mechanism. While the bimodal γ′ microstructure is more resistant and it deforms through precipitate shearing. Viswanathan et al. have studied the effect of cooling rate on the creep deformation in Rene DT88 [5]. Results shows that slow cooled microstructure results in an isolated faulting deformation mode. While the faster cooled microstructure resulted in micro twinning deformation mode and corresponded to a much more creep resistant microstructure. Thus, the creep properties can be improved by modification of the γ′ precipitate microstructure, which is directly determined by the heat treatment [6-9].

According to previous studies, microstructure plays a major role in determining the creep properties and the deformation mode. Therefore, it is important to study the effect of microstructure on the creep properties in order to get more creep resistant microstructure in the newly developed Ni-Co based superalloy.

2 Experiments

The mother ingot of Ni-Co based superalloy with chemical composition listed in Table 1 was prepared by vacuum induction melting (VIM) followed by hot extrusion. The hot extrusion was produced at 1140°C with extrusion ratio of 5.3. After extrusion the alloy was subject to two different heat-treatments to get different microstructures. One was1170 ºC /4h /AC +1080 ºC /4h /AC+845 ºC /24h /AC + 760 ºC /16h /AC to get bimodal sphericalγ′. The other one was1170 ºC /4h /5 °C/min +845 ºC /24h /AC + 760 ºC /16h /AC. In this heat treatment schedule the cooling rate was controlled at 5 °C/min after solution to get large γ′. The specimens for creep tests were cut from the heat treated bars with a gauge length of 25 mm the diameter of 5 mm. Constant-load tensile creep tests were done at 760 °C and 630 MPa. The samples for optical

microscope (OM) observations were etched in a solution of modified Kalling reagent. Polished samples for scanning electron microscope (SEM) observations were electronically etched in 17 ml H_2O 1 ml glacial acetic acid and 2 ml nitric acid solution at 1.5 V for 30 s. Foils for transmission electron microscopy (TEM) observations were prepared by twin-jet thinning technique using a solution of 10 ml perchloric acid and 90 ml alcohol, at a voltage of 20 V, current of 15 mA and temperature of -20 ºC.

3 Results

3.1 Microstructure before creep

Fig. 1 shows the optical microstructure of the alloy after heat-treatment. In order to dissolve all the γ′ into the γ matrix, the solution temperature is higher than the γ′ melting temperature (1118 °C). Therefore the grains grow quickly into a large size (400 μm) for lack of the γ′ precipitate impediment.

Fig. 2 shows SEM image of the samples after different cooling rates. Some MC carbides are still in the grain after both heat treatment schedules. The grain boundary is plain after air cooling, while it is serrate after slow cooling as shown in Fig. 2 and Fig. 3. Previous investigation shows that the degree of the grain boundary serrations is function of the cooling rate. Decreasing the cooling rates results in an increase in the amplitude of serration and our observation is consistent with previous reports. Fan type γ′ is found along the grain boundary in the sample subjected to slow cooling as shown in Fig.3. Fig. 4(a) shows the γ′ morphology in the sample after air cooling. The large spherical γ′ precipitated during air cooling after solution and grew during aging at 1080 °C. The small spherical γ′ precipitated during cooling from 1080 °C and then grew when aged at low temperature. The mean diameter of the large spherical γ′ is 400 nm; and the mean diameter of the small spherical γ′ is 60 nm. Fig. 4(b) shows the γ′ morphology in the sample after slow cooling. The large flowery γ′ formed during slow cooling after solution and the small spherical γ′ formed at low temperature and grew during aging. Obviously, the γ matrix channel between γ′ precipitates is small in the sample subjected to air cooling; by contrast, the γ matrix channel is large in the sample subjected to slow cooling. To sum up, the grain size is similar but the shape of

the grain boundary and the γ′ morphology and distribution are different after two heat treatments.

3.2 Creep curves

Fig. 5 illustrates the creep curves of the alloy subjected to air cooling and slow cooling at 760 °C/ 630 MPa. Fig. 5 shows that the primary stages are short after both heat treatments. Most of the creep strain is accumulated during the accelerating creep stage, however, the creep strain of the alloy after slow cooling increased more rapidly than the one after air cooling. In another word, the creep rate in the alloy after slow cooling is larger than the alloy after air cooling. Therefore, the creep life of the alloy after slow cooling (25 h) is a little shorter than that of after air cooling (32 h), while the alloy after slow cooling possess a larger creep strain (ruptured at 25.9%) than that of after air cooling (rupture at 10.6%).

3.3 The microstructure after creep

Fig. 6 shows the fractograph of the samples after creep rupture. Fig. 6(a) and (b) are the fractograph of the samples subjected to air cooling. Faceted-cleavage is observed as the arrow shows in Fig. 6(a), while river pattern and small quantity of dimples are all observed from Fig. 6(b). Complete dimple-ductile fracture is observed in the sample subjected to slow cooling from Fig. 6(c) and (d) in which the dimple size is nearly 4 μm. In a word, from the fractograph observation, the fracture type of the alloys is different: a quasi-cleavage type fracture in the sample after air cooling and a complete dimple-ductile fracture in the sample after slow cooling.

Fig. 7 shows the creep deformation microstructure after rupture in the sample with air cooling. Fig. 7 (a) is the bright file (BF) image and Fig. 7 (b) is the dark field (DF) image in which the selected area diffraction patterns (SADP) is inserted. Dislocations pileup around the γ′, stacking faults and microtwin are found from Fig. 7 (a). It seems that stacking faults formed only in γ′ and microtwin formed continuously in the γ′ and γ matrix. Fig. 7 (b) shows the dark field image of the microtwin in which the microtwin density is higher than in the bright field image and the microtwins are observed mainly in γ′ phase.

Fig. 8 shows the creep deformation microstructure after rupture in the sample

with slow cooling. It can be seen from Fig. 8 (a) the dislocation density is very high in the sample. Besides the high density dislocation, stacking faults and microtwin are also found. The dislocations mainly pile up around the γ′ phase while the stacking faults and the micro twin continuously penetrate the γ′ phase and the γ matrix. It can be seen that the density of stacking faults and microtwin are very high in γ′ precipitates from Fig. 8 (b). Since the orientations of stacking faults and the micro twin are different there must be two more slip systems started.

4 Discussions

4.1 Effects of the grain boundary

The grain boundary structure is important in determining many mechanical properties, in particular creep and intergranular crack growth [10-12]. From Fig. 2 and Fig. 3 it can be seen that the grain boundaries are serrated after slow cooling. It has been reported that this serrated grain boundary has superior creep damage tolerance compared to planar grain boundaries [11,13,14]. For the serrated grain boundaries are more resistant to the intergranular damage mechanisms. In addition, the formation of the serration reduced the local misorientation between grains. Grain boundary misorientation can be described by the Coincident Site Lattice (CSL) model in which the ∑ number is the reciprocal density of common lattice point along the grain boundary. Lower ∑ orientations, often referred to as 'special' boundary, are known to have much lower energy and diffusive [15]. And growing evidence shows that increasing the fraction of low-∑-oriented boundaries improves creep properties. Low ∑ boundaries are more effective dislocation barriers causing an increase in the matrix-dislocation density and an increase in the internal stress, thereby lower the effective stress [15-17]. Although, lots of evidences show that the serrate grain boundaries are conducive to improving the creep properties, the creep rupture life is still lower in the sampler after slow cooling with serrated grain boundaries. From Fig. 1 it can be seen that the grain size in the sample is as large as 400 μm, and the gauge's diameter of the creep sample is only 5 mm. Therefore, the grain boundaries have no significant effect on the creep properties, while the width of the γ channel and the γ′ morphology are the main reasons for the difference of creep properties [18].

4.2 Effect of the γ channel width

Previous studies show that the volume fraction of the small tertiary γ′ is important for the creep properties of the PM superalloys such as NR3 and Rene DT88 [4, 5, 19]. Actually, the volume fraction of the tertiary γ′ affects the γ channel width which determines the mode of the matrix dislocation propagation. It influences in particular the value of the Orowan stress required to bow out and therefore to propagate the dislocations between the γ′ precipitates. The Orowan stress τ_{or} can be described as following equation:

$$\tau_{or} = 2T / bL \tag{1}$$

Where b is the Burgers vector, T is the line tension of the bowing dislocation and L is the γ channel width. It shows that the Orowan stress is inversely proportional to the γ channel width. In case of the γ channel width is not too small, the a/2<110> dislocation can bow and bypass the γ′ precipitates. On the other hand, when the γ channel width is too small the Orowan stress is very high; as a result, the dislocations must enter into the γ′ particles where they dissociate according to following reaction.

$$\frac{a}{2}[110] \rightarrow \frac{a}{6}[\bar{1}1\bar{2}] + SISF + \frac{a}{3}[211] \tag{2}$$

Therefore, when the γ channel width is small, it is difficult for the dislocations to move through the corresponding microstructure. As Fig. 4 shows the volume fraction of small γ′ is very high after air cooling and the γ channel width is small in this sample, however, the volume fraction of small γ′ is low after slow cooling and the γ channel width is large. According to above analysis, when the γ channel width is small dislocations will cut into the γ′ precipitates for the high Orowan stress, leading to low creep rate and small creep strain. While the γ channel is large dislocations can slip in the matrix and bypass the γ′ precipitates easily, thus the creep rate is high and the creep strain is large in the sample after slow cooling.

4.3 Effect of the γ′ morphology

In the precipitation hardening alloys, the strengthening mechanisms are affected by coherency strains, interfacial energy and morphology, lattice friction stress. Mott

and Nabarro [20] recognize that the strain field resulting from the mismatch between precipitates and the matrix would be a source of strengthening. The strengthening stress is given by

$$\sigma=2G\varepsilon f \quad (3)$$

Where f is the volume fraction of the precipitates and ε is the measure of the stain field which is influenced by the mismatch between precipitates and the matrix. It is common for a coherent precipitates to lose coherency when the particle grows to a critical size. According to Grosdidier et al [21-23] investigation in single nickel based superalloy when the γ′ grow into dendrite morphology the γ′ loss coherency with the γ matrix to make a smoother interface. It is reasonable to consider the flowery γ′ in the sample after slow cooling lose coherency with γ matrix. Therefore the strengthening stress caused by the strain field from misfit between γ′ and γ matrix is disappeared. Thus dislocations can cut into the flowery γ′ more easily than the spherical γ′, just as Fig. 7 and Fig. 8 shows. As a result, the creep rate is higher and the creep strain is larger in the sample after slow cooling. Therefore, the γ′morphology and size should be controlled in order to lower the creep rate.

Conclusion

The creep test of the new developed Ni-Co base superalloy after two different heat treatments were conducted at 760 °C 630 MPa. The effect of heat treatment on the creep performance was discussed and following conclusions were drawn:

(1) The air cooling microstructure, consisting of large spherical γ′ and small spherical γ′, resulted in a slow creep rate and small creep strain. While the slow cooling microstructure, consisting of large flowery γ′ and small spherical γ′, resulted in a fast creep rate and large creep strain.

(2) The γ matrix channel width and the γ′morphology are two main factors for the differences in creep behavior. When the γ channel is large in the slow cooling sample, the dislocations slip and by pass easily, resulting a high creep rate and large creep strain and vice versa for the air cooling sample.

(3) When the γ′ grow into flowery morphology, it loss coherency with the γ matrix. The strengthening from the strain field resulting from the mismatch

between γ′ and γ matrix is disappeared, dislocation cutting into flowery γ′ is more easily than the spherical one.

Acknowledgement

This work was partly supported by Hundreds of Talents Project, National Basic Research Program (973 Program) of China under grant 2010CB631206 and National Natural Science Foundation of China (NSFC) under Grant Nos. 51171179.

Refrence

[1] Y. Yuan, Y. Gu, C. Cui, T. Osada, Z. Zhong, T. Tetsui, T. Yokokawa, H. Harada, Journal of Materials Research, 26 (2011) 2833-2837.

[2] Y. Yuan, Y. Gu, Z. Zhong, T. Osada, T. Yokokawa, H. Harada, in: Superalloys 2012, 2012, pp. 35-42.

[3] Y. Yuan, Y.F. Gu, C.Y. Cui, T. Osada, T. Tetsui, T. Yokokawa, H. Harada, Materials Science and Engineering: A, 528 (2011) 5106-5111.

[4] P.C. D. Locq, S. Raujol, F. Pettinari-Sturmel, A. Coujou, and N. Clément, in: T.M.P. K.A. Green, H. Harada,T.E. Howson, R.C. Reed, J.J. Schirra, and S, Walsto, M.M.S. TMS (The Minerals, 2004 (Eds.) superalloys 2004, 2004, pp. 179.

[5] G.B. Viswanathan, P.M. Sarosi, M.F. Henry, D.D. Whitis, W.W. Milligan, M.J. Mills, Acta Materialia, 53 (2005) 3041-3057.

[6] S.S. Babu, M.K. Miller, J.M. Vitek, S.A. David, Acta Materialia, 49 (2001) 4149-4160.

[7] S. Behrouzghaemi, R.J. Mitchell, Materials Science and Engineering: A, 498 (2008) 266-271.

[8] P. Bhowal, E. Wright, E. Raymond, Metallurgical and Materials Transactions A, 21 (1990) 1709-1717.

[9] J. Mao, K.-M. Chang, W. Yang, K. Ray, S. Vaze, D. Ferrer, Metallurgical and Materials Transactions A, 32 (2001) 2441-2452.

[10] R.J. Mitchell, H.Y. Li, Z.W. Huang, Journal of Materials Processing Technology, 209 (2009) 1011-1017.

[11] A. Wisniewski, J. Beddoes, Materials Science and Engineering: A, 510-511

(2009) 266-272.

[12] A.-C. Yeh, K.-W. Lu, C.-M. Kuo, H.-Y. Bor, C.-N. Wei, Materials Science and Engineering: A, 530 (2011) 525-529.

[13] M.M. H. Loyer Danflou, A. Walder, superalloys 1992, (1992).

[14] R.R. Unocic, N. Zhou, L. Kovarik, C. Shen, Y. Wang, M.J. Mills, Acta Materialia, 59 (2011) 7325-7339.

[15] G. Was, V. Thaveeprungsriporn, D. Crawford, JOM, 50 (1998) 44-49.

[16] V. Thaveeprungsriporn, G. Was, Metallurgical and Materials Transactions A, 28 (1997) 2101-2112.

[17] B. Alexandreanu, B.H. Sencer, V. Thaveeprungsriporn, G.S. Was, Acta Materialia, 51 (2003) 3831-3848.

[18] R.R. Unocic, G.B. Viswanathan, P.M. Sarosi, S. Karthikeyan, J. Li, M.J. Mills. Materials Science and Engineering: A. 483-484 (2008)25-32.

[19 S. Raujol, F. Pettinari, D. Locq, P. Caron, A. Coujou, N. Clément, Materials Science and Engineering A, 387-389 (2004) 678-682.

[20] N.F. Mott, F.R.N. Nabarro, Proceedings of the Physical Society, 52 (1940) 86.

[21 T. Grosdidier, A. Hazotte, A. Simon, Materials Science and Engineering A, 256 (1998) 183-196.

[22] R.A. Ricks, A.J. Porter, R.C. Ecob. Acta Metallurgica. 31 (1983)43-53.

[23] M. Henry, Y. Yoo, D. Yoon, J. Choi. The dendritic growth of γ′ precipitates and grain. Metallurgical and Materials Transactions A. 1993 (24): 1733-1743.

Figure captions

Fig. 1 Optical micrographs of heat-treated microstructure (a) Air cooling; (b) slow cooling

Fig. 2 SEM image of grain boundaries after heat treatment (a) Air cooling; (b) slow cooling

Fig. 3 the fan γ′ along the grain boundary during slow cooling

Fig. 4 γ′ morphology after heat treatment (a) Air cooling; (b) slow cooling

Fig. 5 Creep curves showing plastic strain versus time for the test conditions.

Fig. 6 Fractograph after rupture; (a, b) Air cooling; (c, d) slow cooling

Fig. 7 The deformation microstructure after creep rupture in the alloy with air cooling

Fig. 8 The deformation microstructure after creep rupture in the alloy with slow cooling

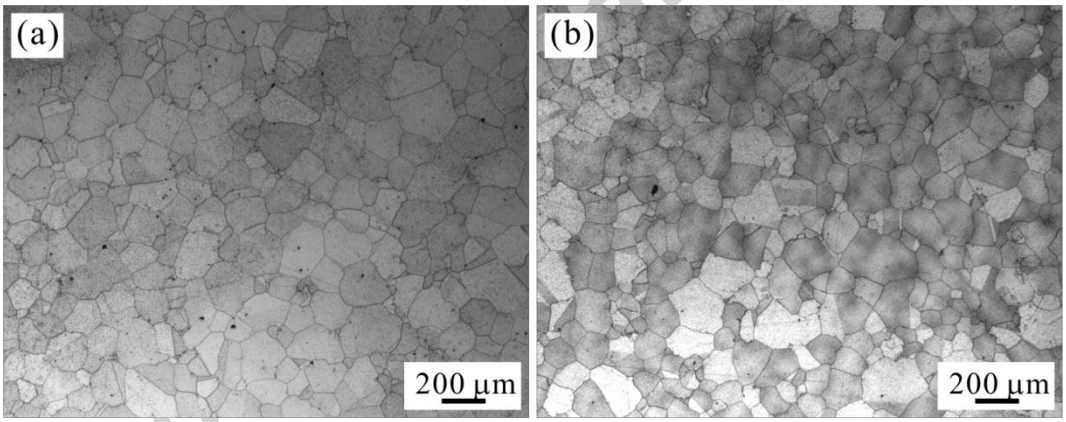

Fig. 1 Optical micrographs of heat-treatedmicrostructure

(a) Air cooling; (b) slow cooling

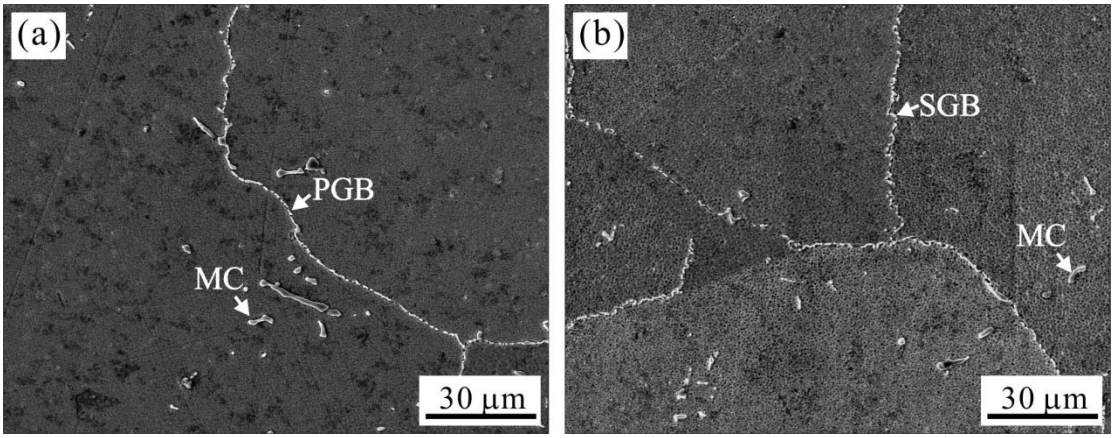

Fig. 2 SEM image of grain boundaries after heat treatment

(a) Air cooling; (b) slow cooling

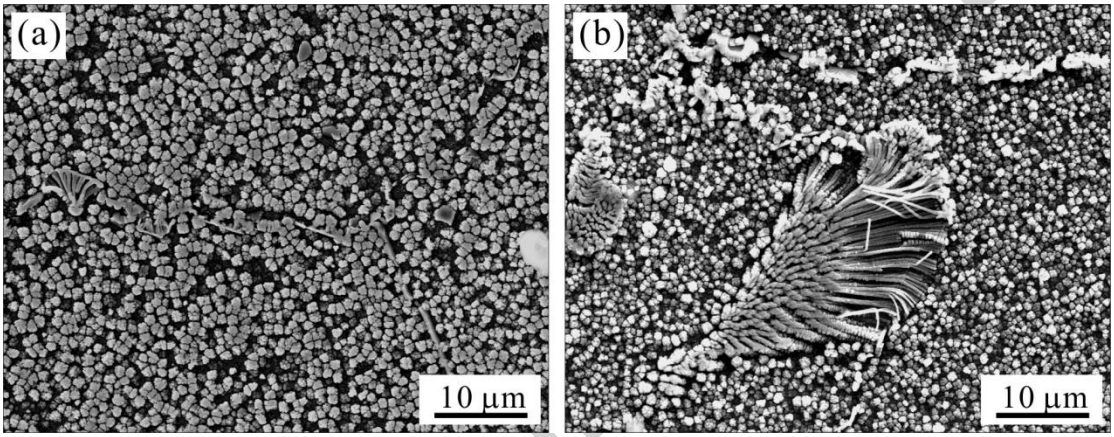

Fig. 3 the fan γ′ along the grain boundary during slow cooling

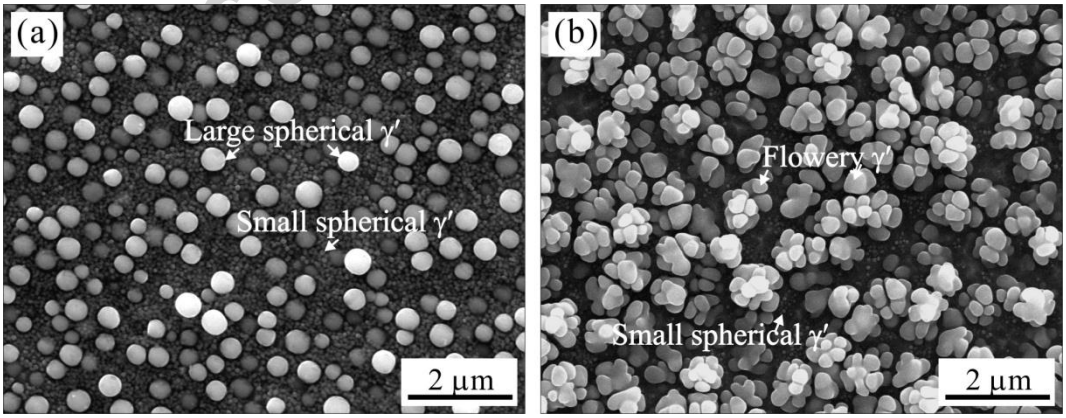

Fig. 4 γ′ morphology after heat treatment

(a) Air cooling; (b) slow cooling

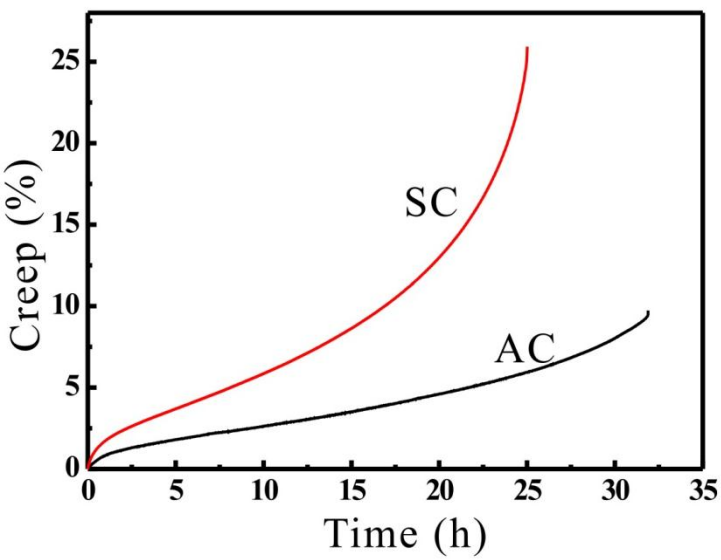

Fig.5 Creep curves showing plastic strain versus time for the test conditions.

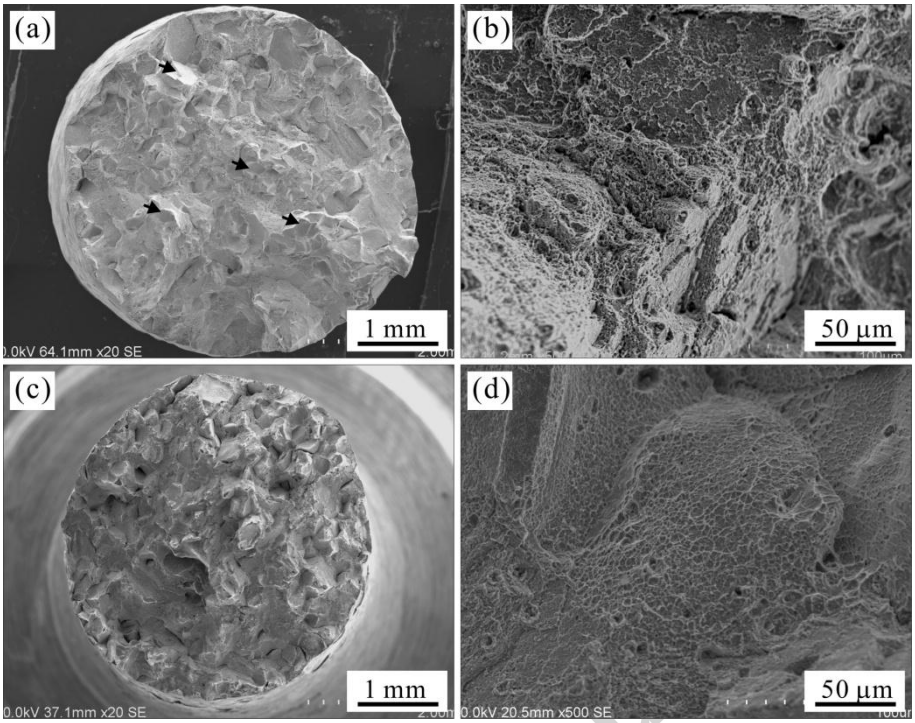

Fig. 6 Fractograph after rupture; (a, b) Air cooling; (c, d) slow cooling

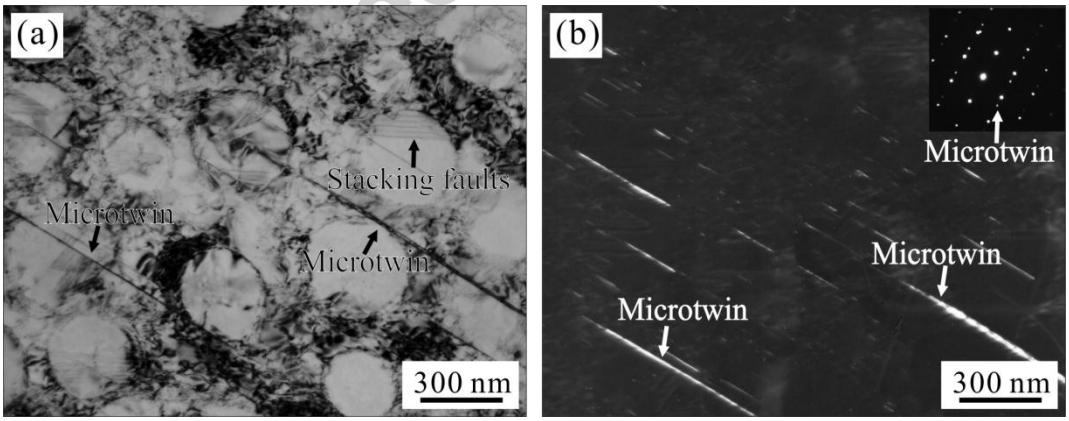

Fig. 7 The deformation microstructure after creep rupture in the alloy with air cooling

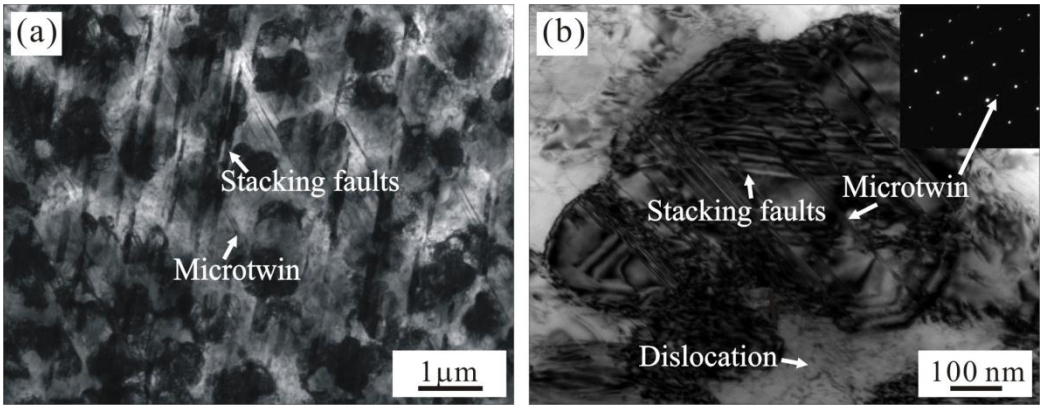

Fig. 8 The deformation microstructure after creep rupture in the alloy with slow cooling

Table 1 Nominal composition of Ni-Co basedsuperalloy (mass fraction, %)

Cr	Co	Mo	Ti	Al	Fe	C	Zr	Ni
14.6	20.5	3.7	5.7	1.9	0.26	0.03	0.05	Bal.